

**Thermographic Evaluation of Aircraft Composite Materials
Paper for WCNDT 08, Shanghai, China**

B. Stephen WONG ¹, Chen Guan TUI ², Weimin BAI ³, Xin WANG ¹

¹Nanyang Technological University, Singapore

²Republic of Singapore Air Force, Singapore

³Formerly with Nanyang Technological University, Singapore

Abstract

This paper will describe and compare the capabilities of various non-destructive thermographic procedures for evaluating defects in aircraft composite materials. The information is derived from joint projects between RSAF and NTU.

Lockin thermography is used by RSAF and other aircraft companies. It involves actively applying sinusoidal thermographic waves to the specimen and observing phase and amplitude changes at the specimen surface in order to evaluate structural information below the surface. Experiments were performed to evaluate defect characteristics such as depth, size and shape. The specimen contained very wide range of delamination defect sizes and depths. Finite Element and theoretical models, which included convection current considerations, were developed and will be presented. These showed good correlation with the experimental results. These models enable optimum frequencies and avoidance of blind frequencies to be predicted.

Also experimental results will be presented using laser thermography which involves controlled heating of the structure surface using a laser and analysis using a thermographic camera.

Finally experimental results will be presented comparing the capabilities of lockin, pulse reflection thermography, though transmission thermography, laser thermography and ultrasonic C scan will be presented.

Keywords: Lock-in thermography, Pulse Thermography, Composites, Laser heating

1. INTRODUCTION

This paper describes experiments conducted using various thermographic non-destructive testing procedures on a carbon fibre composite specimen with delamination defects embedded in it. Lockin thermography evaluations are described which involve experimental, finite element and theoretical models work. This technique is currently being used by RSAF. Other techniques include pulse reflection using a lamp and a laser for heating the specimen. Ultrasonic “C” scan results are also presented. All techniques are compared.

2. SPECIMEN

Carbon-fibre-reinforced plastic (CFRP) specimen

A bi-directional graphite composite specimen with in-planted defects was fabricated and cured in an autoclave.

Size of specimen : 0.3 m x 0.3 m

Number of layers in the specimen : 30

The laminae orientations were 0°/90° crossply throughout the thickness of the specimen. The thickness of each layer was approximately 0.15 mm giving a total specimen thickness of about 4.5 mm.

Defect locations between:

- a) 2nd and 3rd layer (depth 0.3mm)
- b) 4th and 5th layer (depth 0.6mm)
- c) 6th and 7th layer (depth 0.9mm)
- d) 8th and 9th layer (depth 1.2mm)
- e) 10th and 11th layer (depth 1.5mm)
- f) 15th and 16th layer (depth 2.25mm)
- g) 20th and 21st layer (depth 3.0mm)

(As shown in Figure 1)

N. B. In this paper a defect between the 2nd and 3rd layer will be identified as a 2nd layer defect and so on. Therefore defects of sizes 1,2,6,8 and 11 mm in diameter were inserted at each of the above mentioned layers.

Defect material : 3 layers of peel ply

The defects were made by laying the 3 layers of peel ply on top of each other at the appropriate positions during the production of the specimen. The total thickness of the 3 layers together was 0.2mm.

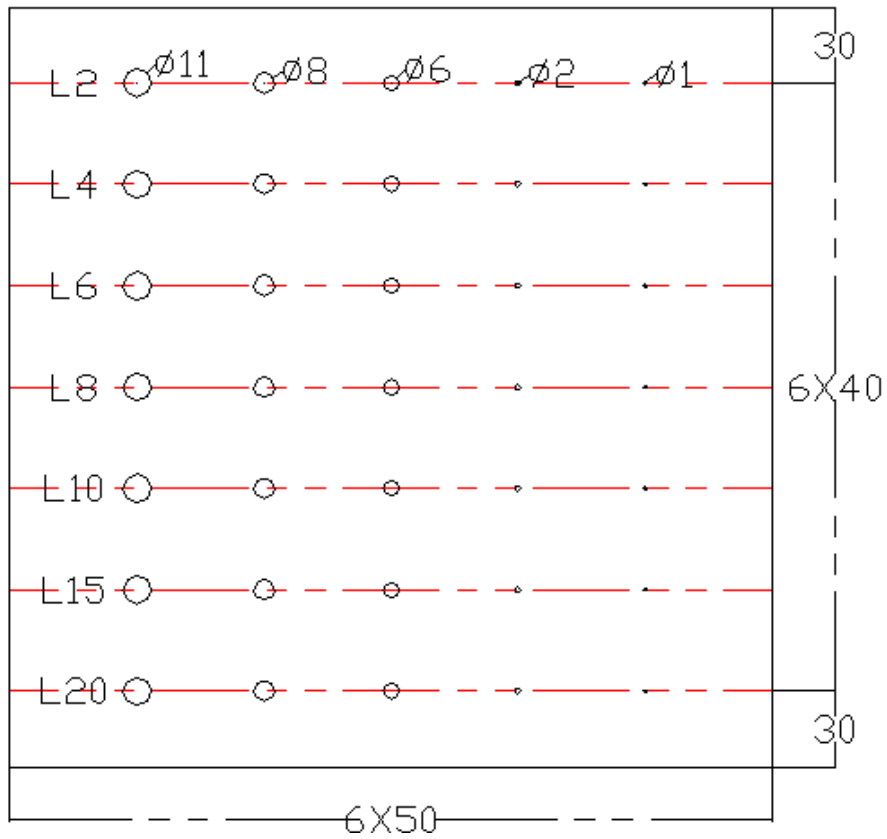


Figure 1. CFRP specimen with in-planted defects of various sizes and locations (Dimensions in mm)

The same specimen was used all for all tests and hence accurate comparisons could be made between the capabilities of the test procedures.

3. EQUIPMENT

3.1 Lock-in thermography equipment

The lock-in thermography system used in this work is an AGEMA Thermovision 900 system. It consists of an infrared camera, a system controller (a computer), a heat source (1 kW-halogen lamp with an infrared filter) and a lock-in module (Figure 2).

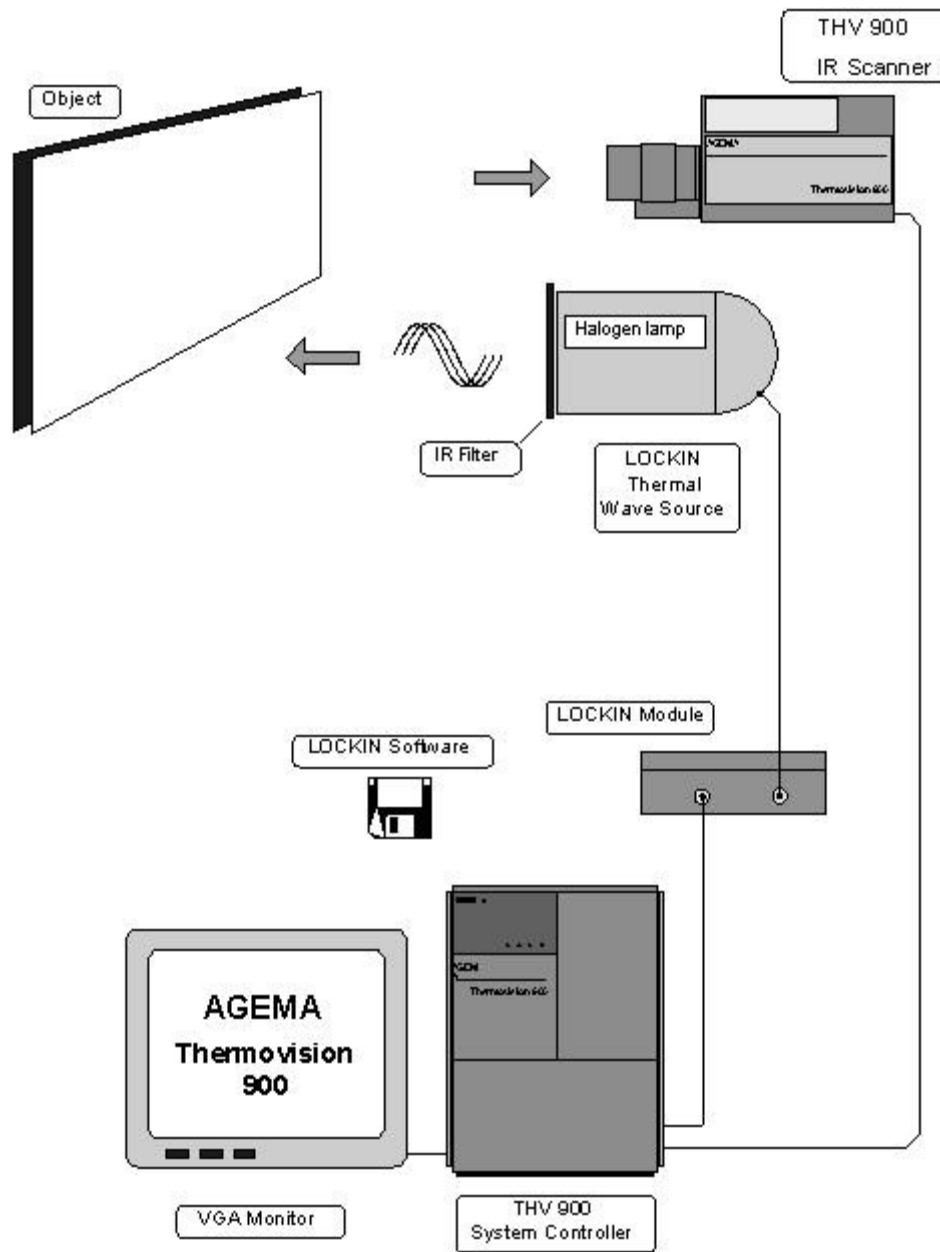


Figure 2. Lock-in system

The heat source is driven by the lock-in module that is controlled by the system controller. As the heat source is modulated digitally, the intensity of the heat source is an approximate sine function. The lock-in module controls the inspection frequency which ranges from 0.0037Hz to 3.75Hz.

During the inspection, the IR camera is used to record the oscillating surface temperature of the inspected object. The image recording is synchronized with the modulation frequency and the IR camera takes 4 images within one cycle (Figure 3). The lock-in

system gets 4 signal values S1, S2, S3 and S4 in every pixel of the image the indices refer to recording time. From these values the system calculates a phase (Φ) image according to the following basic equation:

$$\phi = \arctan \left[\frac{S_1 - S_3}{S_2 - S_4} \right] \quad (1)$$

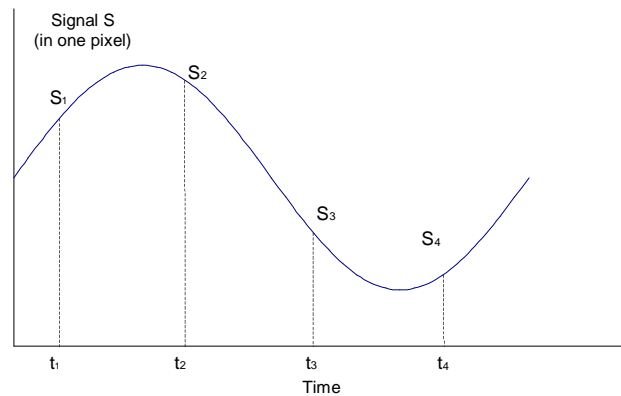


Figure 3. Signal acquisition during thermal wave cycle

All results shown subsequently in this paper concern this phase value which is computed and displayed by the thermographic lockin camera. Another variable magnitude which can also be computed and displayed by the camera. This derived from the square root of the sum of $(S_1 - S_3)^2 + (S_2 - S_4)^2$. The procedure is called lockin magnitude. These are not shown in this paper but some discussion of the data obtained are described in section 5.3.

3.2 Laser system

A general pictorial view shown in Figure 4.



Figure 4. Modu-laser system

The Stella-Pro is the most compact and powerful laser in its class. With the laser tube, power supply, and cooling fans integrated into a single package, the Stellar-Pro is completely self-contained making it extremely compact and efficient. The Stella-Pro has a multi-line outputs delivering up to 230mW of power.

4. EXPERIMENTAL PROCEDURE

4.1 Lock-in thermography

The experiments were performed in a large room and the room temperature was about 23°C. The infrared camera of the lock-in system was positioned at 0.6 metre and perpendicular to the test specimen. The heat source was positioned at 0.5 metro from the specimen. The lens was then focused on the specimen. The specimen was heated to about 80°C with maximum power to shorten the time required to reach the steady state. Subsequently, the specimen was heated periodically at the selected frequency. A steady state was established when the variation of the peak value of the oscillating temperature of the specimen surface was less than 0.5°C. The thermal wave data of the object surface was then collected to produce phase images. The specimen was detected at different modulation frequencies ranging from 0.0037 Hz to 0.93 Hz.

In the room, there was no obvious airflow. Hence the convection occurred at the specimen surface was approximately considered as free convection. In steady state, the average temperature of the front surface was about 75°C and the average temperature of the rear surface was about 71°C. In this situation, convection and radiation occurred simultaneously at the surface of the specimen.

4.2 Pulse reflection thermography

This involves heating the specimen with a heat pulse from the same lamp as used for lockin thermography. The same camera is then used to monitor any changes in temperature of the surface of specimen. Any subsurface defects present may reflect the pulse of heat energy back to the surface. This heats the surface above the defect and hence the presence of the defect is detected.

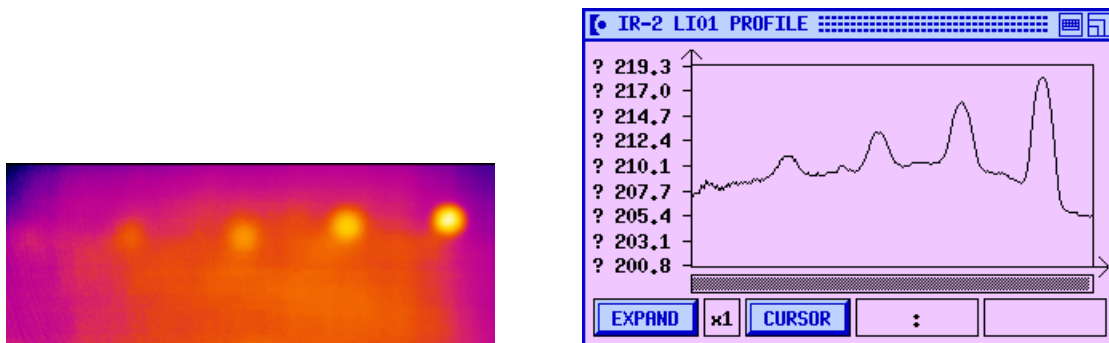
4.3 Laser thermography

The argon laser beam is directly at the CFRP specimen. and the surface temperature monitored with the thermographic camera. Only a small localized area is heated and hence only this small area is assessed. The laser beam is then moved to an adjacent area to monitor this area. If the temperature of the surface rises this is indicative of the presence of a defect for the same reason as mentioned in section 4.2. The camera was fixed at a distance of 1000 mm from the specimen. The distance between the laser and specimen was 150 mm. Only the 11 mm defect at a depth of 0.3 mm was examined.

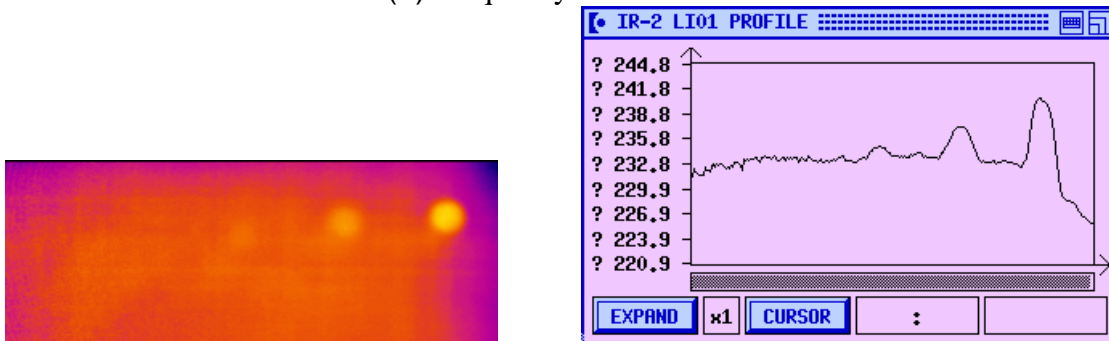
5. RESULTS AND DISCUSSION

5.1 Lock-in thermography - effect of modulation frequency on phase difference produced by defects

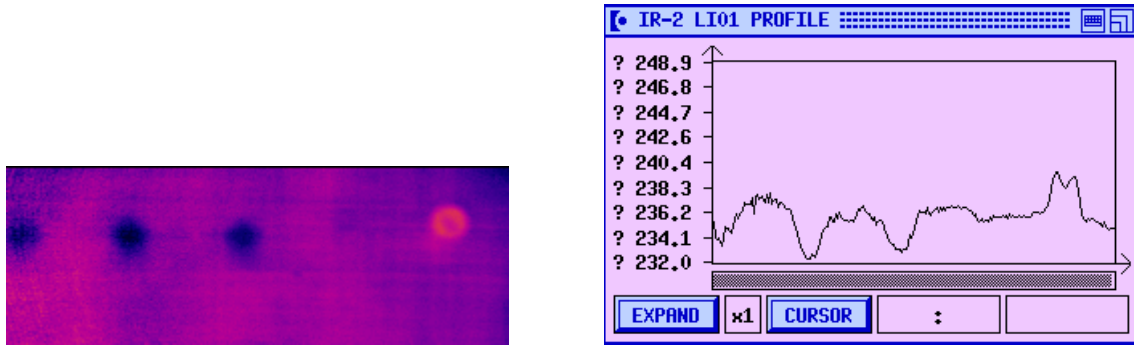
Figure 5 shows some phase images (left) and phase profile plots (right) of the 11 mm defects of the specimen. In the phase images, each pixel represents a phase value related to the phase difference between the oscillating surface temperature and the heat source. From left to right, the depths of the defects are 1.4 mm, 1.12 mm, 0.84 mm, 0.56 mm and 0.28 mm, respectively. The right side images of Figure 5 plot the phase values of a line, which crosses the central points of the 11 mm defect images in the left side phase image. It can be seen that there are phase differences between the defective areas and non-defective areas. Hence the subsurface defects can be detected.



(a) Frequency = 0.0037 Hz



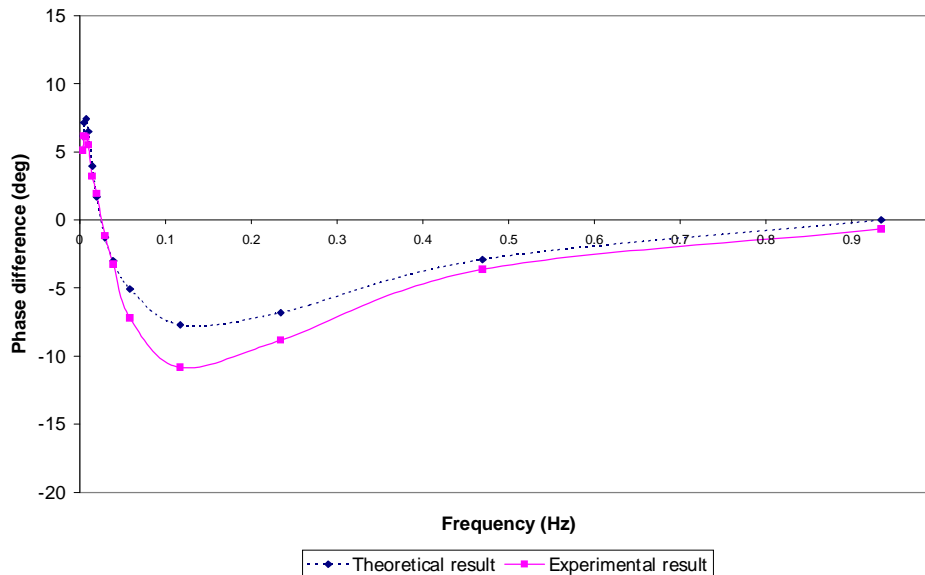
(b) Frequency = 0.0146 Hz



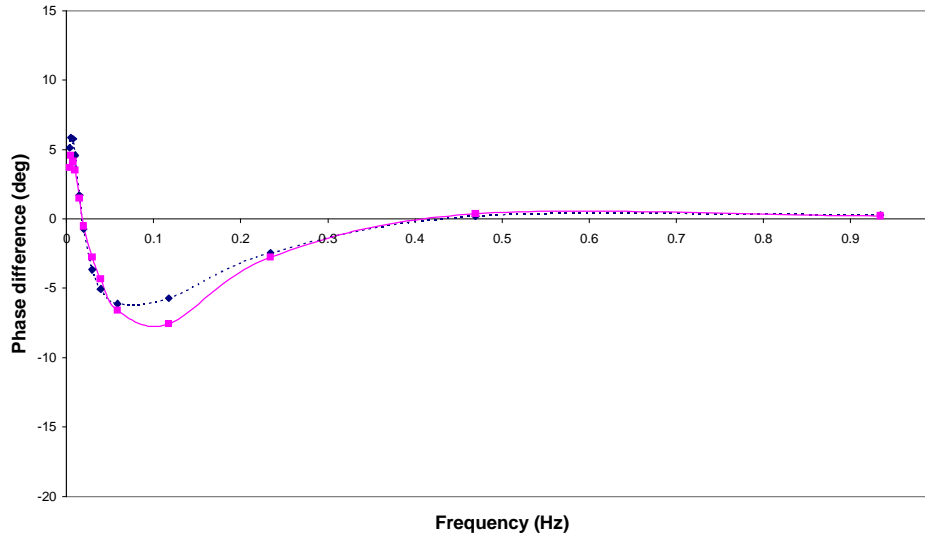
(c) Frequency = 0.0296 Hz

Figure 5. Thermograms and phase profile plots of 11 mm defects

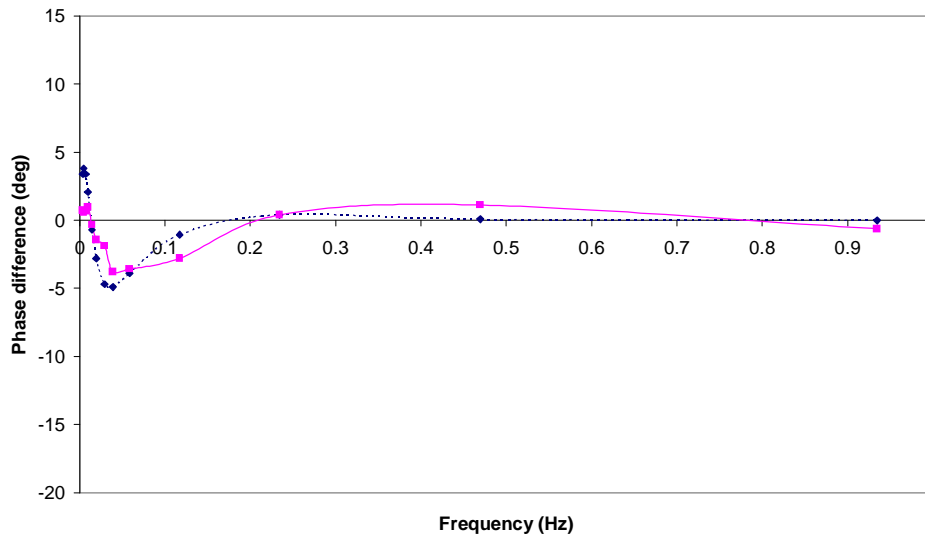
Figure 6 (a) - (c) show the differences between the central point phase values of the 11 mm defects and the average phase values of the non-defective areas. The figures plot both the results obtained from the photothermal model (See Appendix) and the experiment. The figures indicate that the theoretical and experimental results have similar trends. The phase differences obtained experimentally are larger than that obtained theoretically. This is because that there are some air holes in the epoxy resin between the Teflon films. During the fabrication of the specimen, although the autoclave was maintained at high vacuum and the specimen was under high pressure, the air between the Teflon films could not completely escape from the melt epoxy resin. The effective thermal conductivity and density of the epoxy resin with air bubbles are lower than that of pure epoxy.



(a) Defect depth=0.56 mm



(b) Defect depth=0.84 mm



(c) Defect depth=1.4 mm

Figure 6. Phase differences between defective areas and non-defective areas produced by 11 mm defects (theoretical results and experimental results for defects with different depths)

From Figure 6, it can be observed that there exists a frequency for a specific defect at a certain depth such that there is no phase difference or a very small phase difference produced by the defect. Therefore the defect cannot be detected at this frequency, which can be called ‘the blind frequency’. There are another two special frequencies at which a certain defect produces maximum positive or negative phase differences. The two frequencies are

named as the ‘optimum frequencies’. Figure 6 also indicates that the blind frequencies and optimum frequencies change with the defect depths. The deeper the defect depth, the smaller the blind frequency and optimum frequency are.

In practical inspection, the blind frequency should be avoided and the optimum frequencies should be selected. The ‘blind frequencies’ and ‘optimum frequencies’ obtained theoretically are very close to those obtained experimentally. Also, when the size of a laminate shape defect is much larger than the thermal diffusion length, the defect size does not affect the blind frequency and optimum frequency. Hence, the photothermal model described in the Appendix can be used to predict the optimum frequency and blind frequency.

It can also be observed from Figure 6 that the maximum phase differences produced by the defects with the same size decrease with the defect depth. Both the experimental result and theoretical results indicate that the maximum difference produced by an 11-mm defect, which is at a depth of 1.4 mm below the surface, is less than 5 degrees. When the defect depth increases further, the defect cannot be detected.

Finite Element Modeling was also conducted to support the theoretical model. Figure 7 shows the close correlation between the two procedures so FEM provides an effective modeling procedure for Lock-in thermography.

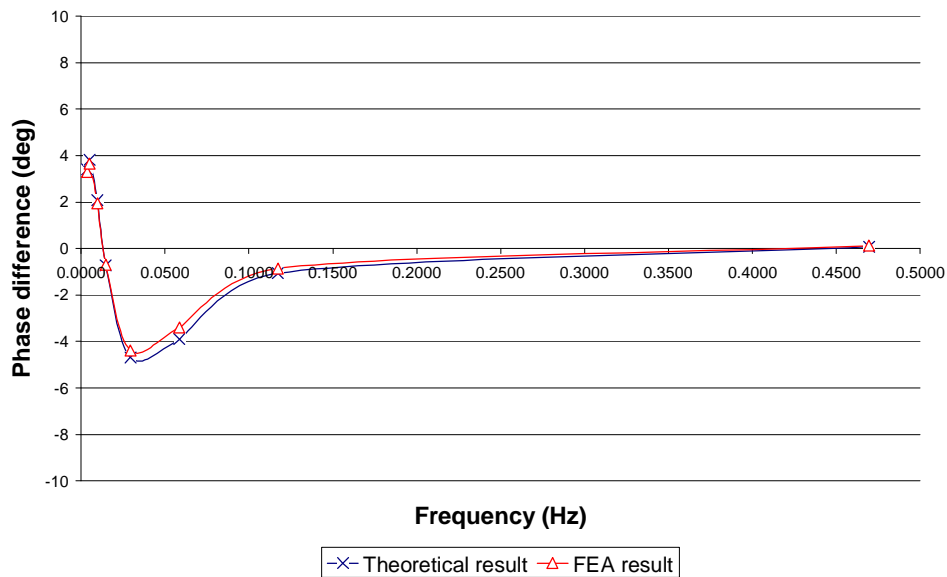


**Figure 7. Comparison between the theoretical and finite element plot
Defect depth=1.4 mm (ref. Figure 8 (c))**

5.2 LASER THERMOGRAPHY RESULTS

Figure 8 shows the result for a non-defective area on the composite specimen. The laser was directed at the specimen heating up just a small area of the specimen. The temperature reaches an equilibrium value of about 54°C after about 8 secs. Figure 9 shows the result by directing the laser beam directly at the known centre of the 11 mm diameter and 0.3 mm deep defect. The temperature reaches an equilibrium value of about 66 °C after about 12 secs. The detected hotter area over the defect clearly indicates the detectability of the defect. A disadvantage is that it takes 12 secs before a reading can be taken.

Figure 10 shows the surface temperatures of the specimen as the laser is moved across the specimen. At each point, the laser was stopped for 3 secs before the temperature was taken. A good temperature contrast is seen for the defect of about 20°C (68 – 48). The defect was also sized quite accurately with the sizing procedure of determining the edge of the defect just before the temperature drops down to the average non-defective area temperature.

Figure 11 shows variation of the surface temperature over the centre of the defect with time using laser and then lamp heating. The heating was started at “4” secs and switched off at “12” secs in both cases. The laser reaches a considerably higher temperature and contrast than the lamp indicating that the laser procedure has greater sensitivity than conventional lamp heated pulse reflection thermography.

Figure 12 shows the surface temperatures of the specimen as the laser is moved across the specimen and also the temperatures using a lamp. The defect only has a contrast of about 3°C compared with the laser of 20 °C again indicating the considerable enhancement of sensitivity using the laser.

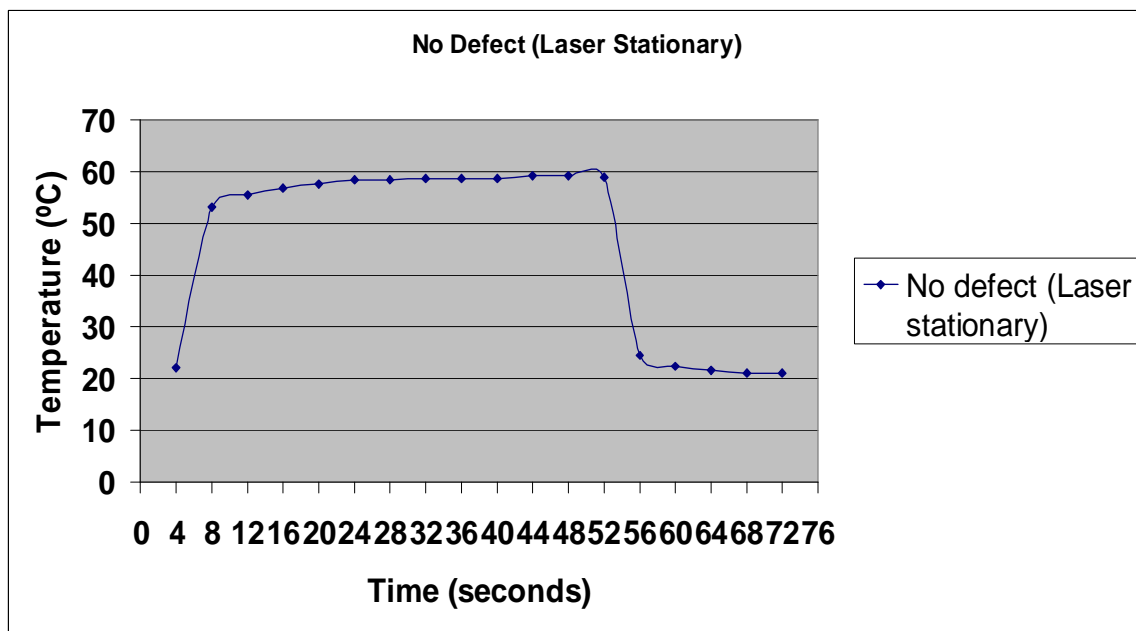


Figure 8. Surface temperature of specimen vs. recording time for a non-defective area

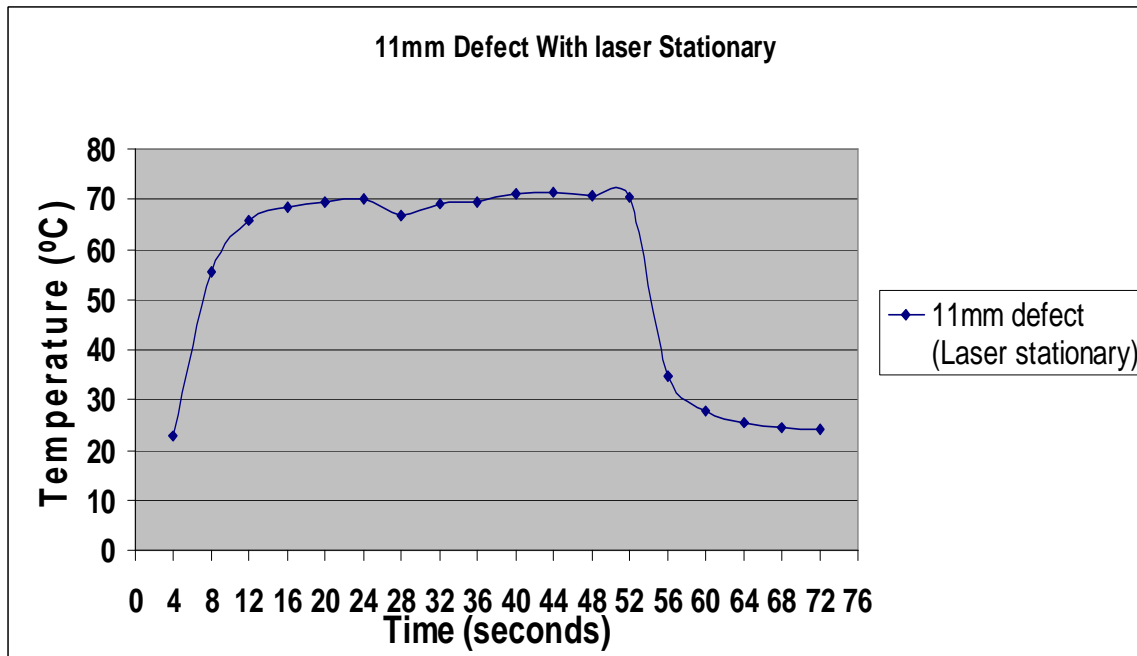


Figure 9. Surface temperature of specimen vs. recording time for a defective area

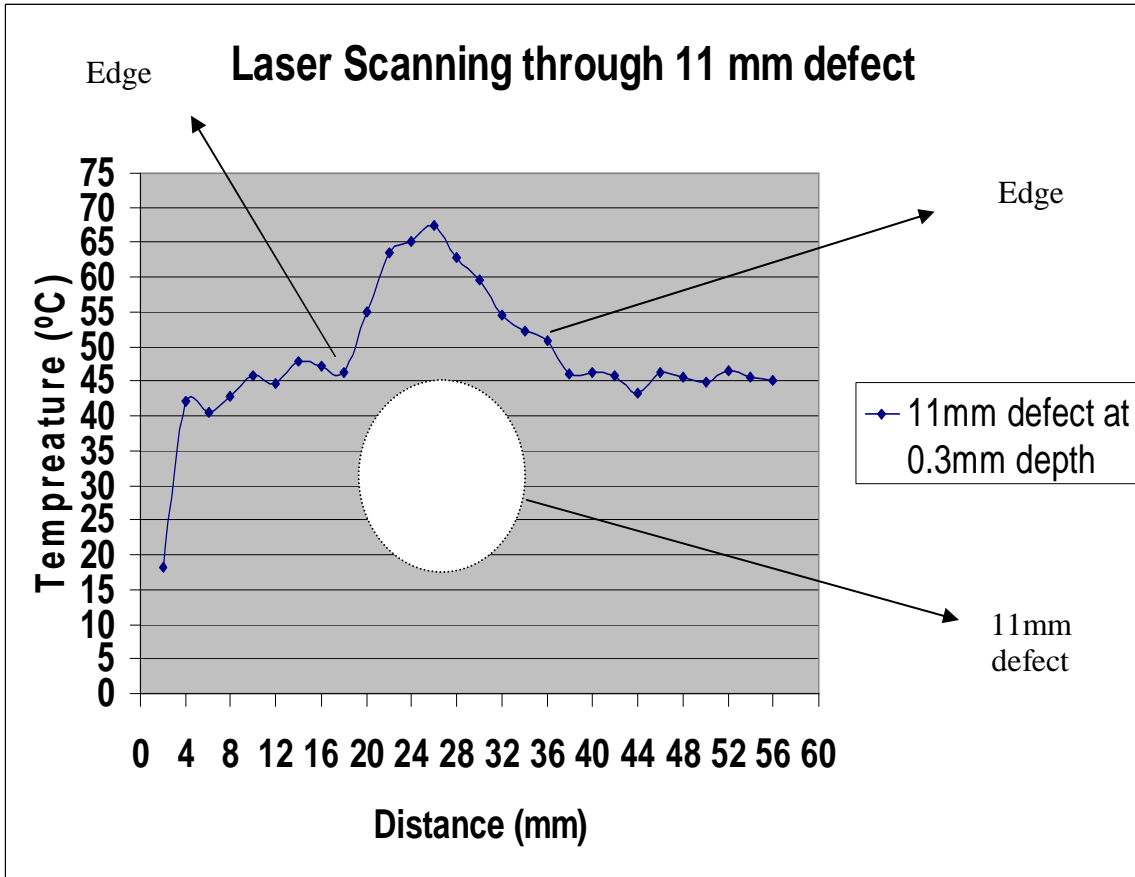


Figure 10. Temperature vs Test distance for the 11 mm diameter defect with a moving laser

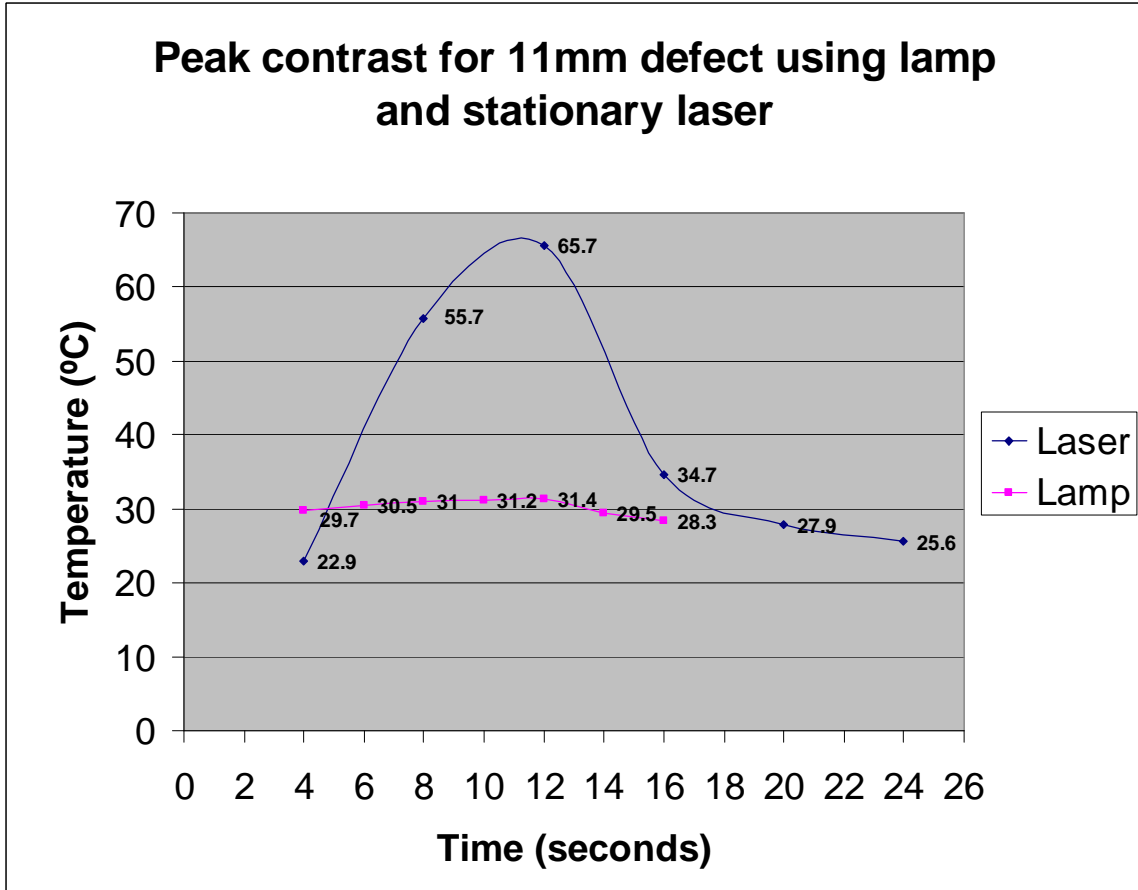


Figure 11. Temperature vs Time for the 11 mm diameter defect using a lamp and stationary laser

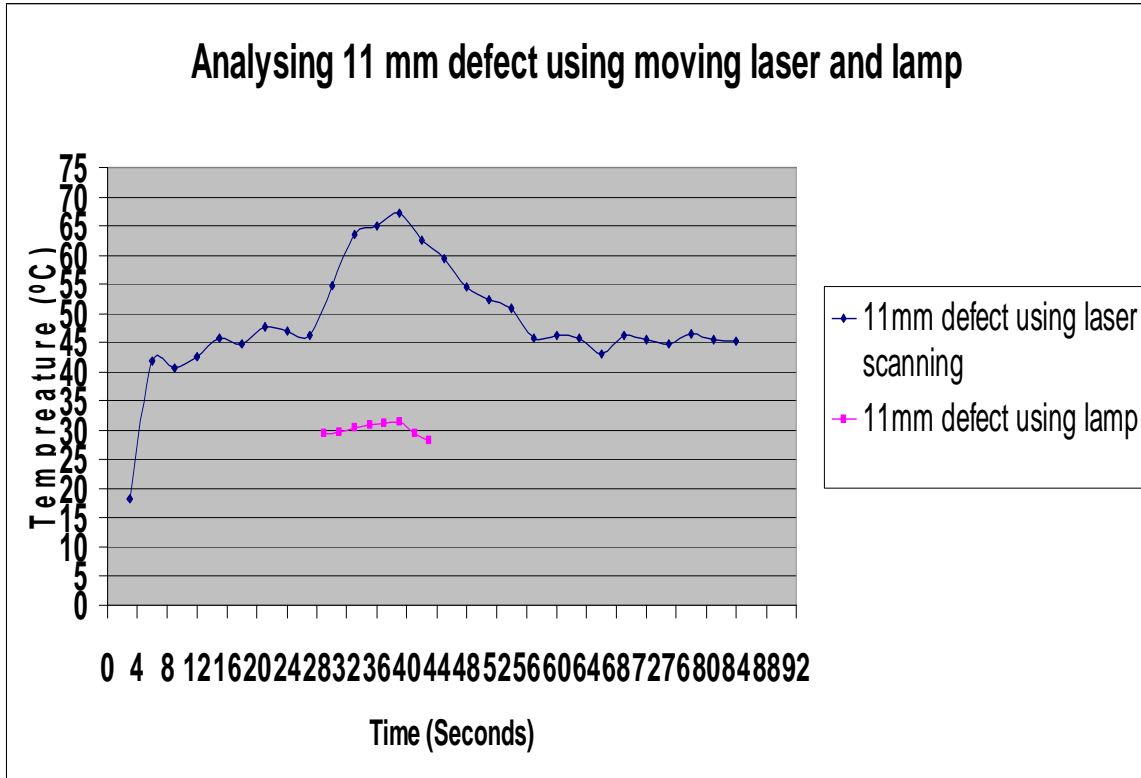


Figure 12. Temperature vs Time for the 11 mm diameter defect using a lamp and stationary laser

5.3 A COMPARISON OF VARIOUS NON-DESTRUCTIVE TESTING TECHNIQUES

Figure 13 shows a comparison of various non-destructive testing techniques on the specimen. The chart shows an approximate experimental comparison only based on whether a defect was detectable or not. The smaller and deeper a defect is, the more difficult it is to detect. Ultrasonic "C" scan is still the most sensitive technique followed by lockin phase thermography, shearography, lockin magnitude and then conventional pulse thermography. The shearography test procedure and results are described in reference 4. The reflection results refer to the procedure which applied a heat pulse to the specimen surface and the defect detected by the heat profile above it. Only the lamp heated pulse reflection are shown since only one defect (the 11mm diameter at 0.3mm) was assessed using laser thermography.

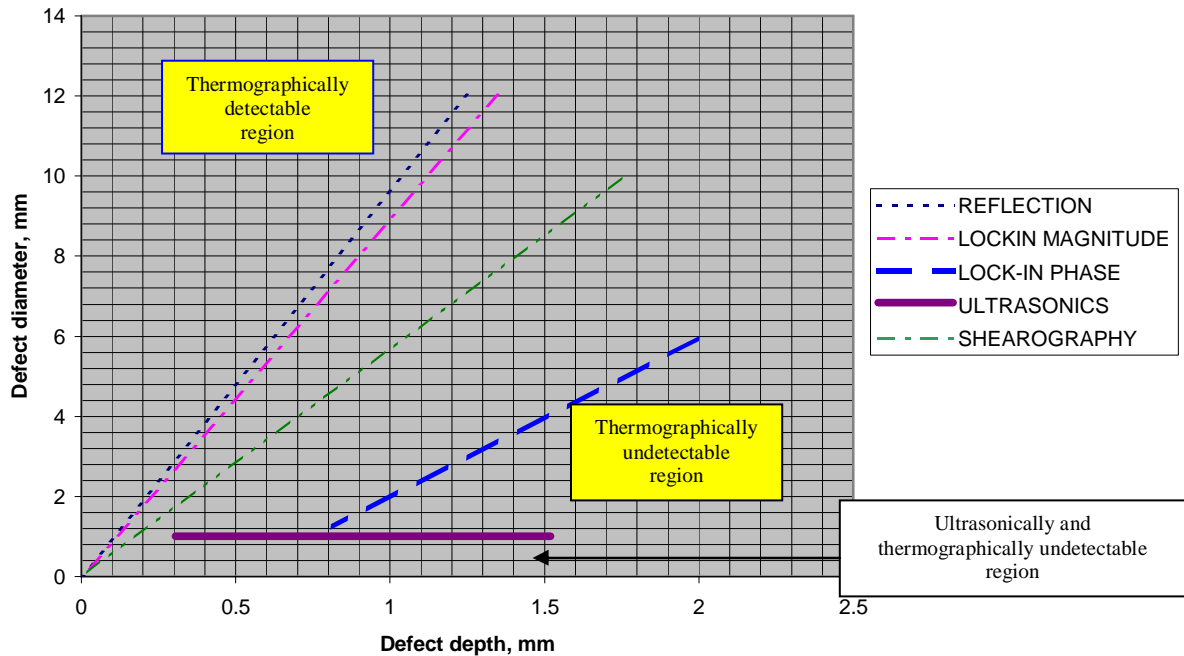


Figure 13. A comparison of various non-destructive testing techniques

6. CONCLUSIONS

Generally the order of defect sensitivity found was "C" scan ultrasonics, lock-in thermography and then shearography. However for near surface defects and for testing thin materials, the latter two techniques are approaching ultrasound's sensitivity. They have the additional advantage of being remote faster techniques and also would be able to test specimens with some slight contours, as in aircraft structures, more effectively.

A theoretical model, finite element modeling and experimental results of lock-in phase thermography showed reasonable close correlation with each other,

The model developed for lock-in phase thermography enables the the optimum frequency for an application to be predicted (i.e. the frequency giving the maximum defect contrast). The blind frequency when no defect can be detected also be predicted. This removes the current trial and error process involved to determine the optimum frequency for testing.

The laser thermography technique was shown to have considerably greater sensitivity for a large defect than the conventional lamp pulse thermography. The disadvantage is the considerably longer time needed for the latter technique since only a small area can be tested at once and a testing time of 3 secs is needed for each small area test.

APPENDIX: THEORY FOR LOCKIN PHASE THERMOGRAPHY ²

An infinitely large multi-layer plate with finite thickness is considered. The plate consists of n thermally different media 1 to n and it is surrounded by air. The different media are separated by planar interfaces (at $x = x_1, x_2, \dots, x_{n-1}$). The thermal properties of the system are labeled: k_i thermal conductivity, ρ_i density, c_i specific heat and α_i thermal diffusivity with $i=1, 2, \dots, n$. A modulated planar heat source is applied to the free surface of medium 1. Medium 1 is the opaque front surface of the plate. The distributed heat flux of the heat source is $(Q_0/2)[1+\cos(\omega t)]$, where Q_0 is the intensity of the heat source, ω is the angular modulation frequency and t is time.

In each layer, the temperature distribution obeys the general heat transfer equation

$$\frac{\partial^2 T_i}{\partial x^2} - \frac{\rho c}{k_i} \frac{\partial T_i}{\partial t} = 0 \quad x_i \geq x \geq x_{i-1} \quad \text{and } i=1 \text{ to } n \quad (\text{A1})$$

where T_i is the temperature in medium i ; the parameter x is perpendicular distance from the front surface and at the front surface x equals to 0.

The front surface is heated by the heat source. At both the front surface and the rear surface convection and radiation occur due to the surface temperature is higher than the environment temperature. Hence, at the two surfaces the boundary conditions are:

$$\begin{aligned} -k_1 \frac{\partial T_1}{\partial x} &= \frac{Q_0}{2} [1 + \cos(\omega t)] - h_f (T_f - T_\infty) \\ &= \text{Re} \left\{ \frac{Q_0}{2} [1 + \exp(j\omega t)] \right\} - h_f (T_f - T_\infty) \quad x=0, t>0 \end{aligned} \quad (\text{A2})$$

$$-k_n \frac{\partial T_n}{\partial x} = h_r (T_r - T_\infty) \quad x=x_n, t>0 \quad (\text{A3})$$

T_f = the temperature of the front surface

T_r = the temperature of the rear surface

T_∞ = the air temperature measured at a point far away from the surfaces

h_f = the heat transfer coefficient of the front surface

h_r = the heat transfer coefficient of the rear surface

At the interfaces between two media, the heat flux is continuous and there exist a thermal contact resistance between the two media. As such, the boundary conditions are:

$$k_i \frac{\partial T_i}{\partial x} = k_{i+1} \frac{\partial T_{i+1}}{\partial x} \quad x = x_i \quad (\text{A4a})$$

$$T_{i+1} - T_i = R_{i,i+1} k_{i+1} \frac{\partial T_{i+1}}{\partial x} \quad (i=1,2,\dots,n-1) \quad (\text{A4b})$$

where, $R_{i,i+1}$ is the thermal contact resistance between medium i and medium $i+1$.

The heat flux is divided into two parts, $Q_0/2$ and $(Q_0/2)\exp(j\omega t)$, which produce a dc temperature increase and an ac thermal modulation respectively. When a steady state is reached, the solution of Equation (1A) has the form:

$$T_i(x, t) = T_{di}(x) + T_{ai}(x) \exp(j\omega t) \quad i = 1, 2, \dots, n \quad (\text{A5})$$

where $T_{di}(x)$ and $T_{ai}(x)\exp(j\omega t)$ are the dc component and the ac component of the temperature in layer i , respectively. In practical inspection, the variation of surface temperature is seldom larger than 10°C . Hence, it is reasonable to assume the heat transfer coefficient as a constant.

As the dc component of the temperature does not change with time, it obeys the following equation:

$$\frac{d^2 T_{di}(x)}{d^2 x} = 0 \quad (\text{A6})$$

subject to the boundary conditions:

$$-k \frac{dT_{di}(x)}{dx} = \frac{Q_0}{2} - h_f(T_{df} - T_\infty) \quad x=0 \quad (\text{A7})$$

$$-k \frac{dT_{di}(x)}{dx} = h_r(T_{dr} - T_\infty) \quad x=x_n \quad (\text{A8})$$

$$k_i \frac{dT_{di}}{dx} = k_{i+1} \frac{dT_{d(i+1)}}{dx} \quad x = x_i, \quad (i=1,2,\dots,n-1) \quad (\text{A9a})$$

$$T_{d(i+1)} - T_i = R_{i,i+1} k_{i+1} \frac{dT_{d(i+1)}}{dx} \quad x = x_i, \quad (i=1,2,\dots,n-1) \quad (\text{A9b})$$

T_{df} = the dc temperature component of the front surface

T_{dr} = the dc temperature component of the rear surface

Because only the ac temperature components are used in lock-in thermography, the primary interest is in the ac component. Substituting Equation (5A) and Equation (6A) into Equation (1A) and omitting the dc component, the following equation is obtained:

$$\exp(j\omega t) \left[\frac{d^2 T_{ai}(x)}{d^2 x} - j\omega \frac{\rho c}{k} T_{ai}(x) \right] = 0 \quad (\text{A10})$$

$$x_i \geq x \geq x_{i-1}, \quad x_0 = 0$$

and the boundary conditions of equation are:

$$-k_1 \frac{dT_{a1}(x)}{dx} = \frac{Q_0}{2} - hT_{af} \quad x = 0, \quad (\text{A11})$$

$$-k_n \frac{dT_{an}(x)}{dx} = hT_{ar} \quad x = x_n \quad (\text{A12})$$

$$k_i \frac{dT_{ai}}{dx} = k_{i+1} \frac{dT_{a(i+1)}}{dx} \quad x = x_i, \quad i = 1, \Lambda, n-1 \quad (\text{A13a})$$

$$T_{a(i+1)} - T_{ai} = R_{i,i+1} k_{i+1} \frac{dT_{a(i+1)}}{dx} \quad x = x_i, \quad i = 2, \Lambda, n-1 \quad (\text{A13b})$$

where

T_{af} = the spatial dependence of the ac temperature component of the front surface

T_{ar} = the spatial dependence of the ac temperature component of the rear surface

The solution of Equation 10A has the following form:

$$T_{ai}(x) = A_i \exp(-\sigma_i x) + B_i \exp(\sigma_i x) \quad (A14)$$

$$\sigma_i = (1 + j) \left(\frac{\omega}{2\alpha_i} \right)^{1/2}, \quad i = 1, 2, \Lambda, n$$

Considering the boundary conditions Equation (11A) to Equation (13A), A_i and B_i can be obtained from the following equation:

$$\begin{bmatrix} k_1\sigma_1+h_f & -k_1\sigma_1+h_f & 0 & 0 & \Lambda & 0 & 0 & 0 & 0 & 0 \\ e^{-\sigma_1 x_1} & e^{\sigma_1 x_1} & (-1-k_2\sigma_2)R_2 e^{-\sigma_2 x_1} & (-1-k_2\sigma_2)R_2 e^{-\sigma_2 x_1} & \Lambda & 0 & 0 & 0 & 0 & 0 \\ k_1\sigma_1 e^{-\sigma_1 x_1} & -k_1\sigma_1 e^{\sigma_1 x_1} & -k_2\sigma_2 e^{-\sigma_2 x_1} & k_2\sigma_2 e^{\sigma_2 x_1} & \Lambda & 0 & 0 & 0 & 0 & 0 \\ 0 & 0 & e^{-\sigma_2 x_1} & e^{\sigma_2 x_1} & \Lambda & 0 & 0 & 0 & 0 & 0 \\ 0 & 0 & k_2\sigma_2 e^{-\sigma_2 x_1} & -k_2\sigma_2 e^{\sigma_2 x_1} & \Lambda & 0 & 0 & 0 & 0 & 0 \\ M & M & O & O & M & O & O & M & M & \bullet \\ 0 & 0 & 0 & 0 & \Lambda & (-1-k_{n-1}\sigma_{n-1})R_{n-2} e^{-\sigma_{n-1} x_{n-2}} & (k_{n-1}\sigma_{n-1})R_{n-2} e^{\sigma_{n-1} x_{n-2}} & 0 & 0 & 0 \\ 0 & 0 & 0 & 0 & \Lambda & -k_{n-1}\sigma_{n-1} e^{-\sigma_{n-1} x_{n-1}} & k_{n-1}\sigma_{n-1} e^{\sigma_{n-1} x_{n-1}} & 0 & 0 & 0 \\ 0 & 0 & 0 & 0 & \Lambda & e^{-\sigma_{n-1} x_{n-1}} & e^{\sigma_{n-1} x_{n-1}} & (-1-k_n\sigma_n)R_{n-1} e^{-\sigma_n x_{n-1}} & (k_n\sigma_n)R_{n-1} e^{\sigma_n x_{n-1}} & 0 \\ 0 & 0 & 0 & 0 & \Lambda & k_{n-1}\sigma_{n-1} e^{-\sigma_{n-1} x_{n-1}} & -k_{n-1}\sigma_{n-1} e^{\sigma_{n-1} x_{n-1}} & -k_n\sigma_n e^{-\sigma_n x_n} & k_n\sigma_n e^{\sigma_n x_n} & 0 \\ 0 & 0 & 0 & 0 & \Lambda & 0 & 0 & (k_n\sigma_n+h_n) e^{-\sigma_n x_n} & -(k_n\sigma_n-h_n) e^{\sigma_n x_n} & 0 \end{bmatrix} \cdot \begin{bmatrix} A_1 & B_1 & A_2 & B_2 & A_3 & \Lambda & B_{n-2} & A_{n-1} & B_{n-1} & A_n & B_n \end{bmatrix}^T = \begin{bmatrix} \frac{Q_0}{2} & 0 & 0 & 0 & 0 & 0 & 0 & 0 & 0 & 0 & 0 \end{bmatrix}^T \quad (A15)$$

At the heated surface (front surface), the spatial dependence of ac temperature component is:

$$T_{af} = T_{ai}(0) = A_1 + B_1 \quad (A16)$$

$$\Phi = \text{Arg}(A_1 + B_1) \quad (A17)$$

Here, A_1+B_1 is a complex quantity. Φ is the phase angle of A_1+B_1 , i.e. the phase difference between the surface temperature and heat source.

For a plate that only has one layer, Equation (15A) becomes

$$\begin{cases} (h_f + k_1\sigma_1)A_1 + (h_f - k_1\sigma_1)B_1 = Q_0 / 2 \\ [(-h_r + k_1\sigma_1) \exp(-\sigma_1 x_1)]A_1 - [(h_r + k_1\sigma_1) \exp(\sigma_1 x_1)]B_1 = 0 \end{cases} \quad (A18)$$

$$A_1 = \frac{Q_0}{2} \cdot \frac{(h_r + k_1\sigma_1) \cdot \exp(2\sigma_1 x_1)}{(h_f + k_1\sigma_1)(h_r + k_1\sigma_1) \cdot \exp(2\sigma_1 x_1) - (h_f - k_1\sigma_1)(h_r - k_1\sigma_1)} \quad (A19)$$

$$B_1 = \frac{Q_0}{2} \cdot \frac{(k_1\sigma_1 - h_r)}{(h_f + k_1\sigma_1)(h_r + k_1\sigma_1) \cdot \exp(2\sigma_1 x_1) - (h_f - k_1\sigma_1)(h_r - k_1\sigma_1)} \quad (A20)$$

and the phase difference between the surface temperature and the heat source is:

$$\phi = \text{Arg} \left[\frac{(h_r + k_1\sigma_1) \cdot \exp(2\sigma_1 x_1) - (h_f - k_1\sigma_1)}{(h_f + k_1\sigma_1)(h_r + k_1\sigma_1) \cdot \exp(2\sigma_1 x_1) - (h_f - k_1\sigma_1)(h_r - k_1\sigma_1)} \right] \quad (A21)$$

This model can be used to predict the phase value caused by a laminate defect. In a plate the area without defect can be considered as a homogeneous plate and the phase value of

non-defective area ($\Phi_{\text{non-defective}}$) can be calculated with Equation (21A). On the other hand, the area with a laminate defect can be considered as a multi-layer structure. The internal layers can be air gaps or other inclusions. The phase value of the defective area ($\Phi_{\text{defective}}$) can be calculated with Equation (17A). The phase difference between the defective area and non-defective area is:

$$\Delta\Phi = \Phi_{\text{defective}} - \Phi_{\text{non-defective}} \quad (\text{A22})$$

h_f , the heat transfer coefficient of the front surface and h_r , the heat transfer coefficient of the rear surface are assumed to be equal for the specimen in this paper and its determination is described in reference (3).

ACKNOWLEDGEMENTS

All the lockin thermography work was conducted by Dr Bai Weimin
The laser thermography work was conducted by Mr Lim Qingwei

REFERENCES

1. Wong, B. S., Tui, C. G., Low, B. S. and Bai, W. "Thermographic and Ultrasonic Evaluation of Composite Materials", *Insight*, UK, Vol. 41, No. 8, pp. 504-509, 1999.
2. Bai. W, and Wong, B. S. "Evaluation of defects in composite plates under convective environments using lock-in thermography", *Measurement Science and Technology*, UK, Vol. 12, pp. 142-150, 2000.
3. Bai. W., and Wong, B. S. "Photothermal models for lock-in thermographic evaluation of plates with finite thickness under convection conditions", *Journal of Applied Physics*, USA, Vol. 89, No. 6, pp. 3275-3282, 2001.
4. Bai. W., Tui, C. G., Wong, B.S. and Murukeshan V. M., "Lockin Thermographic Evaluation Of Composite Materials", *European Conference of Non-Destructive Testing*, Barcelona, Spain, 2002.
5. Lim, Q. "Laser and Thermographic Evaluation of Materials", *Final Year Project*, Nanyang Technological University, MAE, 2007/2008.